LETTERS

Spatially resolved observation of crystal-face-dependent catalysis by single turnover counting

Maarten B. J. Roeffaers[1], Bert F. Sels[1], Hiroshi Uji-i[2], Frans C. De Schryver[2], Pierre A. Jacobs[1], Dirk E. De Vos[1] & Johan Hofkens[2]

Catalytic processes on surfaces have long been studied by probing model reactions on single-crystal metal surfaces under high vacuum conditions. Yet the vast majority of industrial heterogeneous catalysis occurs at ambient or elevated pressures using complex materials with crystal faces, edges and defects differing in their catalytic activity. Clearly, if new or improved catalysts are to be rationally designed, we require quantitative correlations between surface features and catalytic activity—ideally obtained under realistic reaction conditions[1–3]. Transmission electron microscopy[4–6] and scanning tunnelling microscopy[7,8] have allowed *in situ* characterization of catalyst surfaces with atomic resolution, but are limited by the need for low-pressure conditions and conductive surfaces, respectively. Sum frequency generation spectroscopy can identify vibrations of adsorbed reactants and products in both gaseous and condensed phases[9], but so far lacks sensitivity down to the single molecule level. Here we adapt real-time monitoring of the chemical transformation of individual organic molecules by fluorescence microscopy[10–12] to monitor reactions catalysed by crystals of a layered double hydroxide immersed in reagent solution. By using a wide field microscope, we are able to map the spatial distribution of catalytic activity over the entire crystal by counting single turnover events. We find that ester hydrolysis proceeds on the lateral {10$\bar{1}$0} crystal faces, while transesterification occurs on the entire outer crystal surface. Because the method operates at ambient temperature and pressure and in a condensed phase, it can be applied to the growing number of liquid-phase industrial organic transformations to localize catalytic activity on and in inorganic solids. An exciting opportunity is the use of probe molecules with different size and functionality, which should provide insight into shape-selective or structure-sensitive catalysis[13–15] and thus help with the rational design of new or more productive heterogeneous catalysts.

The present study used [Li^+-Al^{3+}] layered double hydroxide (LDH) catalysts, which are composed of linked octahedrons of aluminium hydroxide. The octahedrons form gibbsite-type sheets stacked in a hexagonal space group, resulting in prismatic crystals with large basal {0001} planes[16] (Fig. 1a). The occupation of two out of three octahedrons by Al^{3+} and the presence of Li^+ in the residual octahedrons result in a positive charge on the layers. This feature endows the solid with anion exchange capacity, with exchanged anions such as OH^- located in the galleries between the sheets and at the gallery entrances located at the {10$\bar{1}$0} crystal faces.

Because our experiments require large crystals with easily-identifiable faces, we used [Li^+-Al^{3+}] LDH, which readily forms such crystals. (The LDHs and their thermal treatment products used as adsorbents, drug delivery vehicles, polymer stabilizers and catalysts usually have other compositions[17–20].) Scanning electron microscopy on hydrothermally prepared LDH samples shows flat, well-defined crystals with smooth basal planes. There are frequently intergrowths at the {0001} planes. Typically, the $(0001)'$ plane of the intergrowing component is slightly tilted with respect to the (0001) plane of the underlying crystal component (Fig. 1b).

Processes such as molecular motor movements and enzyme dynamics have been visualized at the single-molecule level[10,21] using fluorescent probes. Here we modify the recent work[11,12] that monitored the hydrolytic activity of individual lipase B enzymes of *Candida antarctica* with the fluorogenic probe 5-carboxyfluorescein diacetate (C-FDA). Like other non-fluorescent esters of fluorescein such as fluorescein diacetate (FDA), C-FDA becomes emissive only upon catalytic hydrolysis in water-containing media, or upon catalytic transesterification with, for example, 1-butanol (Fig. 1a). In this study, a wide field fluorescence microscope was used to map the catalytic activity of the LDH crystals dispersed in milli-Q water (18 MΩ resistance) and deposited through spin coating on cleaned cover glasses. The cover glasses were then mounted at the bottom of a 1,000 μl reaction chamber, which allows exposure of the LDH crystals to the fluorogenic reagent solution while monitoring the fluorescence signal of the product in inverted microscope mode (Fig. 1a).

In a first control experiment, an amine-functionalized glass slide was used to catalyse the reaction of C-FDA with 1-butanol. The glass surface was exposed for 1 h to a 1:1,000,000 mixture of N,N-dimethylaminopropyltrimethoxysilane (DMAPTS) and propyltrimethoxysilane (PTS) in $CHCl_3$, and the functionalized surface thoroughly rinsed (three times) with $CHCl_3$. For optimal observation of catalytic events, we used an excitation power of 4 kW cm^{-2} as a good compromise between sensitivity and enhanced product bleaching. Upon addition of the non-fluorescent C-FDA precursor to the reaction chamber, bright spots appear owing to the formation of single molecules of emissive fluorescein (Fig. 2a). Photobleaching causes rapid disappearance of the spots (usually within 1 s) and thus prevents the rapid accumulation of background fluorescence. No spots were detected at all within the same time window when a clean glass slide replaced the catalyst, or when only propyl groups were anchored to the surface. Increasing the DMAPTS to PTS ratio during the glass surface preparation to 1:10,000 increases the concentration of catalytic sites, as evidenced by the larger density of fluorescent spots observed (Fig. 2b–d); quantification of the fluorescent signal suggests a 20-fold increase in the transesterification rate. When preparing this catalytic surface, part of the active surface monolayer was mechanically removed; in these defunctionalized zones, no spots are visible. Clearly, the formation of fluorescent molecules is directly related to the presence of catalytically active basic sites.

Next, LDH crystals were studied with the {0001} plane parallel to the cover glass. The catalytic activity of this class of catalysts is known to increase with surface area; based on combined CO_2 chemisorption

[1]Microbial and Molecular Systems, Katholieke Universiteit Leuven, Kasteelpark Arenberg 23, B-3001 Leuven, Belgium. [2]Division of Molecular and Nano Materials, Katholieke Universiteit Leuven, Celestijnenlaan 200F, B-3001 Leuven, Belgium.

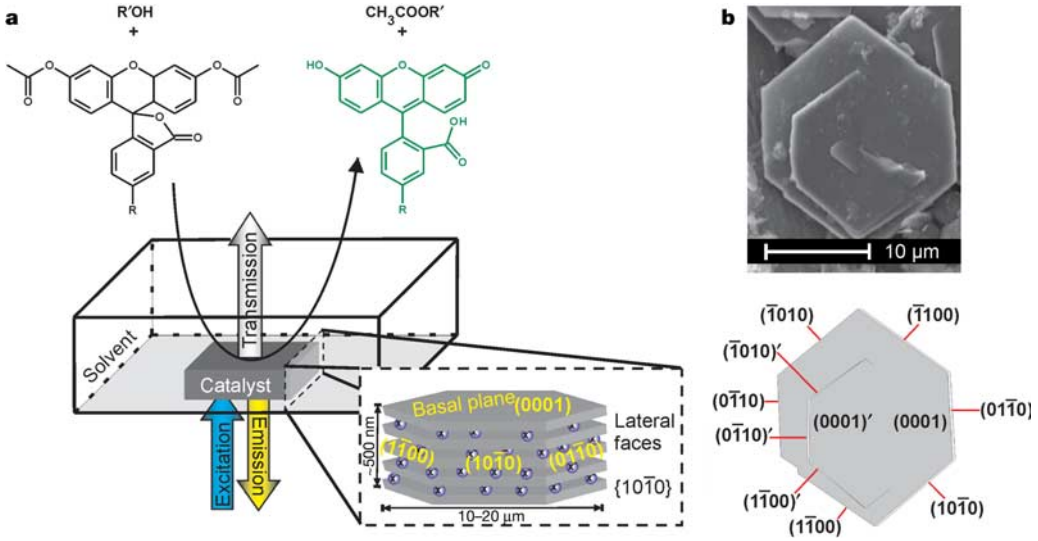

Figure 1 | Experimental set-up. a, Schematic drawing of the experimental set-up: the LDH particle is exposed to fluorescein ester (R = –COOH for C-FDA; R = –H for FDA) in R′OH solution (R′ = –H for hydrolysis; R′ = $-nC_4H_9$ for transesterification). A wide field microscope with 488 nm excitation light was used. The inset shows the different crystallographic faces of a hexagonal LDH crystallite with indication of the Miller indices. **b**, Scanning electron micrograph of a typical LDH crystal with assignment of the different crystal faces for the intergrown crystal.

and kinetic catalytic data, it has been suggested that only a small fraction of the sites are responsible for the activity, and that these most active sites are probably situated at the edges and corners of the crystallites, or at the gallery entrances[20,22,23]. Figure 1 illustrates catalytic sites located on the {0001} basal surface of the LDH crystal, and OH^- ions at the {10$\bar{1}$0} faces, which in the two-dimensional projection of the microscopic image appear at the edge of the hexagonal crystals. When carrying out transesterification of C-FDA in 1-butanol, spots appear all over the basal surface without preference for crystal edges (Fig. 3a, b, d). No fluorescence signal is detected in the solution surrounding the crystal, demonstrating that transesterification in this system is indeed catalysed by LDH in a true heterogeneous fashion. We also studied ester hydrolysis by using an aqueous reaction medium instead of an alcohol solvent (Fig. 1a), observing fluorescent spots primarily at the crystal edges and less at the basal surface (Fig. 3e). The fluorescence intensity distribution obtained when accumulating observations of the same crystal over 256 images clearly indicates that the hydrolysis activity follows the contours of the crystal (Fig. 3f, h). The activity of base catalysis by LDH is thus not always associated with the same type of sites: whereas transesterification occurs mainly at the {0001} plane, hydrolysis requires the {10$\bar{1}$0} faces where exchanged OH^- ions at the entrance of the galleries may be the active species. Such information has so far only been obtained very indirectly; for example, by correlating trends in catalytic activity with *ex situ* physical characterization of the catalyst samples used[22,23]. Our *in situ* fluorescence approach, in contrast, has sufficient spatial resolution to allow us to simultaneously observe the activity associated with different crystal faces and thus uncover different reactive centres for two distinct base-catalysed reactions in the same crystal.

Time-dependent experiments permit determination of diffusion and reaction rates. For the reaction of 40 nM C-FDA with 1-butanol (Fig. 3a), counting the spots appearing on the basal plane reveals a typical transesterification rate of 4.2 molecules per 100 μm^2 over a period of 96 ms, corresponding to $(7.2 \pm 0.4) \times 10^{-13}$ mol m^{-2} s^{-1} (Fig. 3c). With 600 nM C-FDA the number of spots increases and yields a rate of $(1.0 \pm 0.1) \times 10^{-11}$ mol m^{-2} s^{-1}. Recording of rates for reagent concentrations between 0 and 700 nM (Fig. 3b) proves that in this range, the reaction is first order in reagent (data not shown). When FDA is used as the substrate for the transesterification reaction, a slightly lower rate of $(2.5 \pm 0.5) \times 10^{-13}$ mol m^{-2} s^{-1} for 100 nM FDA is measured (see Supplementary Video 3). We attribute this difference to the extra carboxylate group of C-FDA, which leads to a higher concentration of adsorbed substrate at the positively charged surface, and hence to higher reaction rates. For the transesterification, the rates measured on {0001} are in fair agreement with transesterification rates measured for bulk LDH samples, which typically have surface areas between 50 and 250 m^2 g^{-1} (refs 24–27).

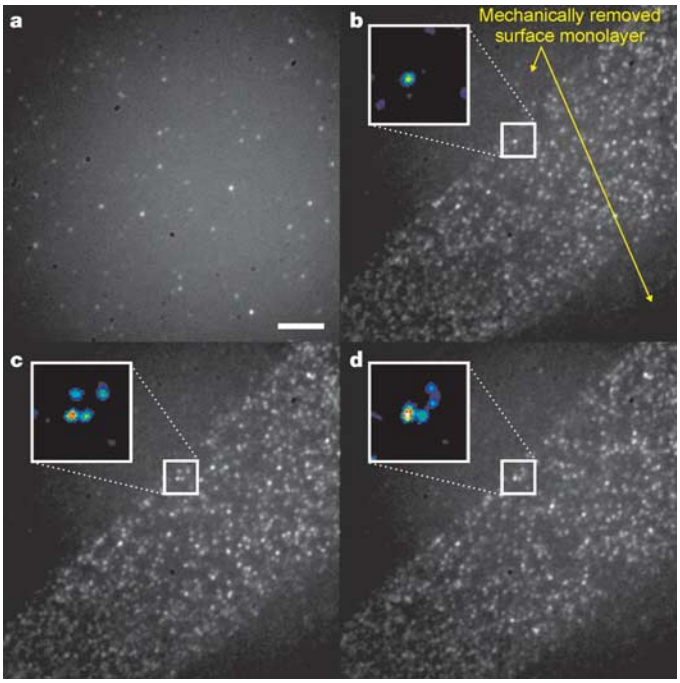

Figure 2 | *In situ* wide field fluorescence micrographs of C-FDA transesterification on propyl amine-functionalized cover glasses. a, Image of a cover glass functionalized with 1:1,000,000 DMAPTS:PTS mixture. Newly formed product molecules appear as bright spots, which are bleached soon after. Scale bar, 5 μm. **b**, Same reaction, on a cover glass prepared with 1:10,000 DMAPTS:PTS mixture. In the uniformly black zones, surface functionalization was mechanically removed. The insets show the formation of individual molecules in a 2.5 × 2.5 μm^2 square (see Supplementary Video 1). **c**, **d**, same as **b** but 96 and 192 ms later. Reactions were carried out at room temperature with 450 nM C-FDA in pure 1-butanol.

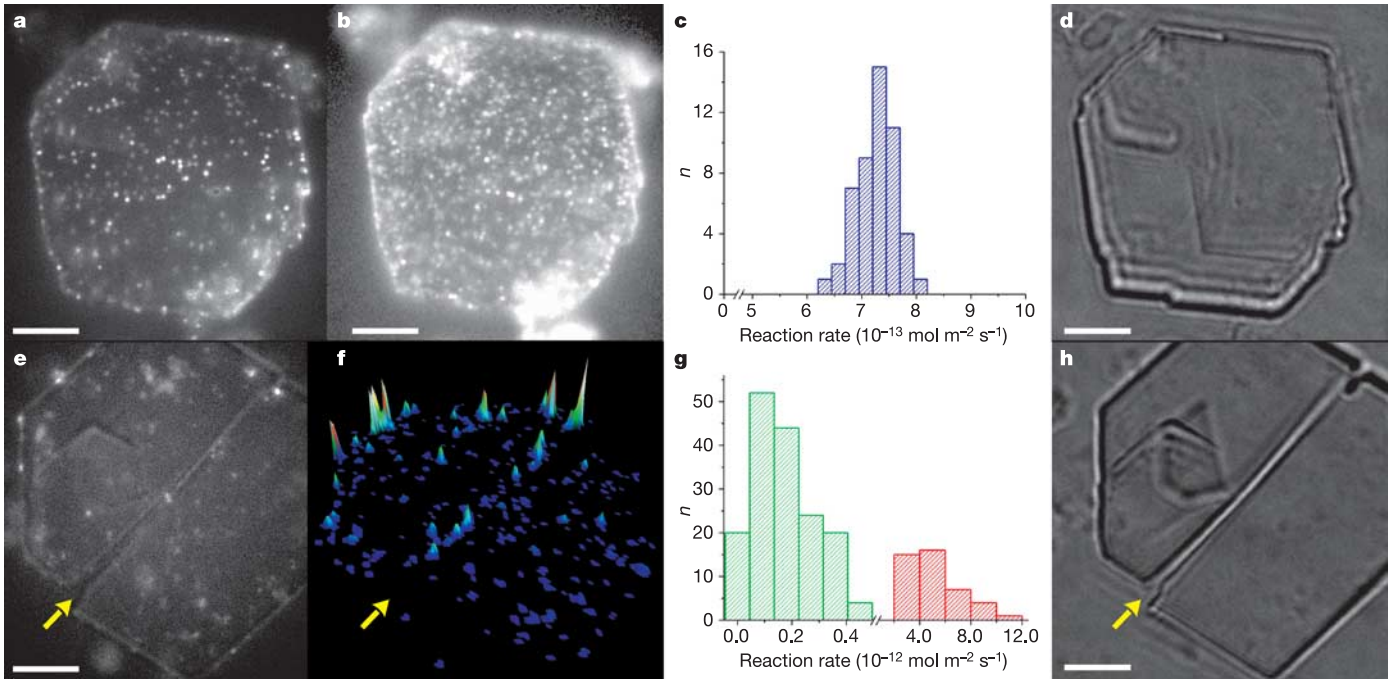

Figure 3 | Wide field images of catalytic reactions on individual LDH particles. **a**–**d**, Transesterification of C-FDA with 1-butanol at 40 nM (**a**) and 700 nM (**b**) ester concentration on the same LDH crystal (see Supplementary Video 2). **c**, Distribution of initial reaction rates for 1 μm^2 domains on the crystal faces ($n = 50$). **d**, Transmission image of the crystal. **e**–**h**, Hydrolysis of 600 nM C-FDA on an LDH crystal. **e**, Fluorescence image, showing formation of single product molecules mainly at crystal edges (96 ms per image). **f**, Accumulated spot intensity on the same crystal over 256 consecutive images. **g**, Distribution of initial reaction rates for 1 μm^2 domains on the faces of the LDH crystal ($n = 207$). The distribution clearly shows two statistically different subpopulations. The fast population corresponds to active domains located on the $\{10\bar{1}0\}$ faces (red), whereas the {0001} faces host the slow population (green). **h**, Transmission image. Scale bars, 5 μm. Yellow arrows in **e**, **f**, **h** indicate the same viewing direction on the same crystal.

For the hydrolysis of C-FDA (600 nM) on an LDH catalyst particle, the contributions of the different crystallographic planes can be clearly separated (Fig. 3g). Spots formed on the $\{10\bar{1}0\}$ faces of either the main crystal or intergrown crystals correspond to at least 85% of the overall activity of the particle. On the {0001} plane, the hydrolysis rate is only $(1.7 \pm 1.2) \times 10^{-13}$ mol m^{-2} s^{-1} for 600 nM C-FDA, while at the $\{10\bar{1}0\}$ faces the rate averages to $(4.7 \pm 2.3) \times 10^{-12}$ mol m^{-2} s^{-1}. Counting of single turnovers thus allows us to quantify the heterogeneity in reaction kinetics at the level of individual crystal faces, thus providing important information that could aid the design of industrial catalysts with improved activity.

Close inspection of the Supplementary videos reveals motion of the fluorescent dots. This allows us to monitor the diffusion of the fluorescent products of the transesterification reaction along the large {0001} crystal face over several time frames, before bleaching occurs (Fig. 4). The displacements $|r|$ travelled between the observations by many product molecules can be adequately fitted as $f(r) = (2r/\langle r^2 \rangle) \exp[-r^2/\langle r^2 \rangle]$, with $\langle r^2 \rangle$ the mean square displacement[28]. From this a diffusion coefficient, D, can be calculated, based on $D = \langle r^2 \rangle / 4t$ and with $t = 96$ ms. We find that over 90% of the 5-carboxyfluorescein product molecules are highly mobile, with $D = (3.0 \pm 0.5) \times 10^{-14}$ m^2 s^{-1}. A small fraction of the product molecules is almost immobile, with $D \leq 1 \times 10^{-16}$ m^2 s^{-1}. The diffusion of dye molecules trapped in mesoporous siliceous materials exhibits a similar bimodal behaviour, with fast-moving as well as stationary molecules[28]. In the case of fluorescein dye, a diffusion coefficient of $D = (3.0 \pm 0.5) \times 10^{-14}$ m^2 s^{-1} was measured for more than 80% of the molecules, while $D \leq 7 \times 10^{-16}$ m^2 s^{-1} for the rest of the molecules. Catalyst deactivation by strong product adsorption is known in basic catalysis, and we are currently investigating whether the immobile molecules are related to this phenomenon.

Extending and improving the use of *in situ* fluorescence microscopy as a tool for probing heterogeneous catalysis calls for better spatial resolution, and for the availability of probe molecules that can be used to monitor a wide range of different chemical reactions. We anticipate that spatial resolution might be improved by an order of magnitude by future advances in fluorescence microscopy, such as STED (stimulated emission-depletion) methods[29]. We have also already identified suitable probes for base-, acid- and metal-catalysed reactions, such as ester exchange, Friedel-Crafts or hydrogenation reactions. In a first extension of the present work, we have mapped the spatial distribution of Friedel-Crafts catalytic activity in the channels of a mordenite zeolite crystal (see Supplementary Information). We anticipate that reporter probes with different size and functionality could be used to gain insight into steric, electronic and polarity characteristics of reactive sites. We expect that such developments, used in conjunction with methods for characterizing the inorganic catalyst material, will provide better insight into challenging aspects of heterogeneous catalysis, such as shape-selective[13] and key-lock[30] catalysis in zeolites, or structure-sensitive catalysis on supported metals[14,15].

METHODS

Materials. $[LiAl_2(OH)_6]^+OH^- \cdot nH_2O$ was hydrothermally synthesized following a reported procedure[31]. A toluene solution of 35 μmol Al tri-*sec*-butoxide was added dropwise to an aqueous solution of LiOH (Al/Li = 1.5). Gels were treated hydrothermally for 10 d at 403 K. Products were washed with hot water to eliminate the excess lithium salts. Crystallinity and crystal size were checked using scanning electron microscopy and X-ray diffraction (hexagonal unit cell parameters: $a = 5.09$ Å and $c = 15.2$ Å). Pure, large hexagonal LDH crystals were obtained, with smooth basal planes about 10–20 μm in diameter and a characteristic thickness of about 500 nm. As only OH^- ions are available during synthesis, the LDH is completely in the OH^- form.

Observation of catalytic processes. The wide field microscope consists of an inverted microscope (IX-71, Olympus) with a 100×, 1.3 NA oil immersion

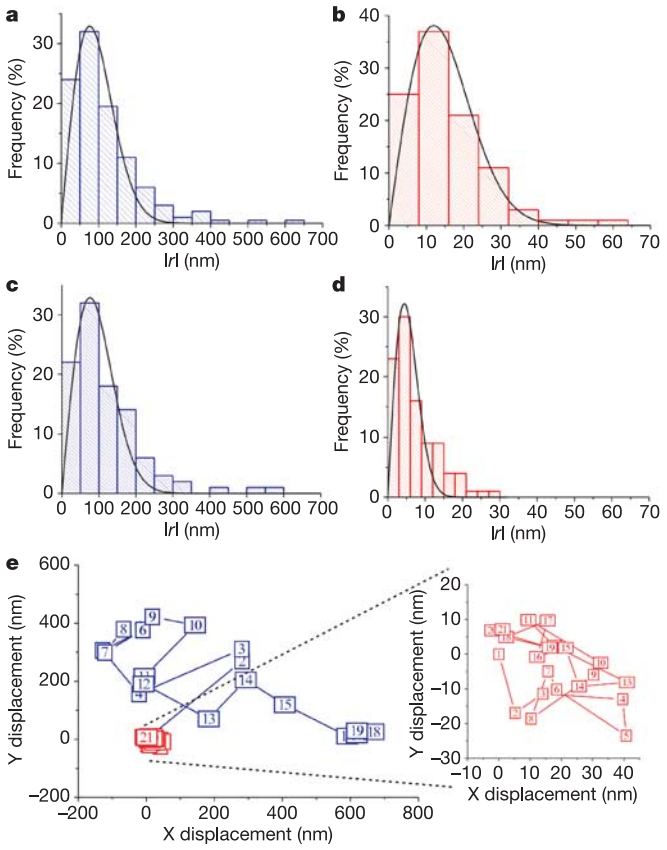

Figure 4 | Analysis of single product molecules randomly diffusing on (0001) LDH surfaces after transesterification. The time lag between the frames is 96 ms (see Supplementary Video 4). **a**, **b**, The distribution ($n = 100$) of step sizes r for fluorescein shows two different populations. **a**, Over 80% of the molecules show a high mobility with a mean displacement of more than 100 nm. **b**, For a small group of molecules, the displacement is of the same order as the positioning accuracy (~10 nm). **c**, **d**, As in **a**, **b**, but with 5-carboxyfluorescein, produced from C-FDA. **e**, The trajectories of two representative fluorescein molecules (red: stationary; blue: highly mobile; same colours as histograms in **a** and **b**). Numbers in **e** represent consecutive positions of the molecules. Reactions were carried out at room temperature with 40 nM C-FDA or 100 nM FDA in pure 1-butanol.

objective lens and a highly sensitive cooled Electron Multiplying-CCD (cascade 512B, Princeton Instruments Inc.). The wide field illumination was achieved by focusing the expanded circular polarized 488 nm light from an Ar^+ laser (Stabilite 2017, Spectra-Physics) onto the back focal plane of the objective. Emission is collected by the same objective and imaged by the CCD after passing through a dichroic mirror and spectral filters removing the excitation light. The image was expanded 3.3 × before the CCD, resulting in a field of view of 24.2 × 24.2 μm. Transmission images were obtained by Köhler illumination.

Received 14 June; accepted 8 November 2005.

1. Thomas, J. M. & Thomas, W. J. *Principles and Practice of Heterogeneous Catalysis* (Wiley-VCH, Weinheim, 1996).
2. Thomas, J. M. Catalysis and surface science at high resolution. *Faraday Discuss.* **105,** 1–31 (1996).
3. Ertl, G., Knözinger, H. & Weitkamp, J. *Handbook of Heterogeneous Catalysis* (Wiley-VCH, Weinheim, 2000).
4. Hansen, T. W. *et al.* Atomic-resolution in situ transmission electron microscopy of a promoter of a heterogeneous catalyst. *Science* **294,** 1508–1510 (2001).
5. Hansen, P. L. *et al.* Atom-resolved imaging of dynamic shape changes in supported copper nanocrystals. *Science* **295,** 2053–2055 (2002).
6. Helveg, S. *et al.* Atomic-scale imaging of carbon nanofibre growth. *Nature* **427,** 426–429 (2004).
7. Zambelli, T., Barth, J. V., Wintterlin, J. & Ertl, G. Complex pathways in dissociative adsorption of oxygen on platinum. *Nature* **390,** 495–497 (1997).
8. Wolff, J., Papathanasiou, A. G., Kevrekidis, I. G., Rotermund, H. H. & Ertl, G. Spatiotemporal addressing of surface activity. *Science* **294,** 134–137 (2001).
9. Dellwig, T., Rupprechter, G., Unterhalt, H. & Freund, H. J. Bridging the pressure and materials gap: High pressure sum frequency generation study on supported Pd nanoparticles. *Phys. Rev. Lett.* **85,** 776–779 (2000).
10. Lu, H. P., Xu, L. & Xie, X. S. Single-molecule enzymatic dynamics. *Science* **282,** 1877–1882 (1998).
11. Velonia, K. *et al.* Single-enzyme kinetics of CALB-catalyzed hydrolysis. *Angew. Chem. Int. Edn Engl.* **44,** 560–564 (2005).
12. Flomenbom, O. *et al.* Stretched exponential decay and correlations in the catalytic activity of fluctuating single lipase molecules. *Proc. Natl Acad. Sci. USA* **102,** 2368–2372 (2005).
13. Corma, A. Inorganic solid acids and their use in acid-catalyzed hydrocarbon reactions. *Chem. Rev.* **95,** 559–614 (1995).
14. Boudart, M., Aldag, A., Benson, J. E., Dougharty, N. A. & Harkins, C. G. On the specific activity of platinum catalysts. *J. Catal.* **6,** 92–99 (1966).
15. Bernasek, S. L., Siekhaus, W. J. & Somorjai, G. A. Molecular-beam study of hydrogen-deuterium exchange on low- and high-Miller-index platinum single-crystal surfaces. *Phys. Rev. Lett.* **30,** 1202–1204 (1973).
16. Fogg, A. M., Freij, A. J. & Parkinson, G. M. Synthesis and anion exchange chemistry of rhombohedral Li/Al layered double hydroxides. *Chem. Mater.* **14,** 232–234 (2002).
17. Cavani, F., Trifiro, F. & Vaccari, A. Hydrotalcite-type anionic clays: preparation, properties and applications. *Catal. Today* **11,** 173–301 (1991).
18. Cai, H., Hillier, A. C., Franklin, K. R., Nunn, C. C. & Ward, M. D. Nanoscale imaging of molecular adsorption. *Science* **266,** 1551–1555 (1994).
19. Sels, B. *et al.* Layered double hydroxides exchanged with tungstate as biomimetic catalysts for mild oxidative bromination. *Nature* **400,** 855–857 (1999).
20. Sels, B. F., De Vos, D. E. & Jacobs, P. A. Hydrotalcite-like anionic clays in catalytic organic reactions. *Catal. Rev.* **43,** 443–488 (2001).
21. Noji, H., Yasuda, R., Yoshida, M. & Kinosita, K. Direct observation of the rotation of F1-ATPase. *Nature* **386,** 299–302 (1997).
22. Roelofs, J. C. A. A., Lensveld, D. J., van Dillen, A. J. & de Jong, K. P. On the structure of activated hydrotalcites as solid base catalysts for liquid-phase aldol condensation. *J. Catal.* **203,** 184–191 (2001).
23. Abelló, S. *et al.* Aldol condensations over reconstructed Mg-Al hydrotalcites: structure–activity relationships related to the rehydration method. *Chem. Eur. J.* **11,** 728–739 (2005).
24. Corma, A., Iborra, S., Miquel, S. & Prim, J. Production of food emulsifiers, monoglycerides, by glycerolysis of fats with solid base catalysts. *J. Catal.* **173,** 315–321 (1998).
25. Engel, D. J., Malloy, T. P., & Nickl, P. K. Transesterification using metal oxide solid solutions as the basic catalyst. US Patent 5,350,879 (1993).
26. Watanabe, Y. & Tatsumi, T. Hydrotalcite-type materials as catalysts for the synthesis of dimethyl carbonate from ethylene carbonate and methanol. *Micropor. Mesopor. Mater.* **22,** 399–407 (1998).
27. Abelló, S. *et al.* Aldol condensations over reconstructed Mg–Al hydrotalcites: structure–activity relationships related to the rehydration method. *Chem. Eur. J.* **11,** 728–739 (2005).
28. Hellriegel, C., Kirstein, J. & Bräuchle, C. Tracking of single molecules as a powerful method to characterize diffusivity of organic species in mesoporous materials. *N. J. Phys.* **7,** 1–14 (2005).
29. Hell, S. W. Toward fluorescence nanoscopy. *Nature Biotechnol.* **21,** 1347–1355 (2003).
30. Martens, J. A. *et al.* Evidences for pore mouth and key–lock catalysis in hydroisomerization of long n-alkanes over 10-ring tubular pore bifunctional zeolites. *Catal. Today* **65,** 111–116 (2001).
31. Serna, C. J., Rendon, J. L. & Iglesias, J. E. Crystal-chemical study of layered $[Al_2Li(OH)_6]^+X^-.nH_2O$. *Clays Clay Miner.* **30,** 180–184 (1982).

Supplementary Information is linked to the online version of the paper at www.nature.com/nature.

Acknowledgements M.B.J.R. thanks the Institute for the Promotion of Innovation through Science and Technology in Flanders (IWT-Vlaanderen) for a fellowship, B.F.S. thanks the FWO-Flanders for a post-doctoral fellowship and the KUL for a guest professor position. This work was performed within the framework of the IAP-V-03 programme 'Supramolecular Chemistry and Catalysis' of the Belgian Federal government and of GOA-2/01.

Author Information Reprints and permissions information is available at npg.nature.com/reprintsandpermissions. The authors declare no competing financial interests. Correspondence and requests for materials should be addressed to D.E.D.V. (dirk.devos@biw.kuleuven.be) or J.H. (johan.hofkens@chem.kuleuven.be).